Construction and Building Materials 346 (2022) 128494

Contents lists available at ScienceDirect

Construction and Building Materials

journal homepage: www.elsevier.com/locate/conbuildmat

Effect of the expanded perlite dose on the fire performance of gypsum plasters

Marcos Lanzón [a,*], Francisco José Castellón [b], Manuel Ayala [b]

[a] Departamento de Arquitectura y Tecnología de la Edificación, Escuela Técnica Superior de Arquitectura y Edificación, Campus Paseo Alfonso XIII 50, 30203, Universidad Politécnica de Cartagena, Spain
[b] Departamento de Estructuras, Construcción y Expresión Gráfica, Campus Muralla del Mar, Doctor Fleming s/n., 30202, Universidad Politécnica de Cartagena, Spain

ARTICLE INFO

Keywords:
Lightweight plasters
Expanded perlite
Fire protection
Characterisation

ABSTRACT

Gypsum plasters are often used in buildings to provide passive protection against fire. This paper studies the fire behaviour of lightweight plasters containing moderate and high doses of expanded perlite. A propane flame was used to study the heat transmission through the plaster from the exposed side to the back side (2 cm thickness) using an IR camera. The microstructural and mineralogical variations induced by fire were analysed by scanning electron microscopy (SEM), X-ray diffraction (XRD), thermogravimetric analysis (TGA) and differential scanning calorimetry (DSC) using micro-perforated lids to improve the resolution (separation) of endothermic peaks of gypsum and bassanite. The exposed side of the plasters was drastically affected by fire regardless the concentration of perlite. However, important differences were found in the non-exposed side depending on the used amount of perlite. The greatest alteration was observed for high doses of perlite (6.5 % w/w) followed by control samples (0 % w/w). By contrast, using moderate doses of perlite (2.0 % w/w) the plasters showed excellent fire performance and $CaSO_4$ $2H_2O$ was well preserved. The results suggest that the incorporation of lightweight materials to plasters should be carefully adjusted to ensure appropriate fire protection.

1. Introduction

Gypsum ($CaSO_4$ $2H_2O$) is a non-combustible material coded as A1 by the EN 13501–1 (gypsum binder for direct use) standard [1]. For this reason, gypsum plasters have been widely used to provide building materials with passive protection against fire [2,3]. The crystallisation water in gypsum delays the temperature increase as part of the heat energy is absorbed by the mineral to produce bassanite ($CaSO_4$ $½H_2O$) and, finally, anhydrite at higher temperatures ($CaSO_4$). After total dehydration, the material still behaves as a passive element due to the incombustible nature of $CaSO_4$ and no harmful gases or smoke are emitted.

Expanded perlite is a low-density aggregate used in a wide variety of building materials like plasters and renders [4]. The incorporation of lightweight aggregates, such as expanded perlite may improve specific properties of cementitious materials. Usually, expanded perlite decreases the material's mechanical performance with the increase of the aggregate due to air cavities of perlite [5–14]. However, the pozzolanic activity of perlite powder can be beneficial for the mechanical strength of cements, concrete and mortars [15–19]. Another advantage of using expanded perlite in building materials is the lower thermal conductivity and heat transfer caused by perlite pores (air) [10,20–23], affecting the fire behaviour of plasters. Besides, expanded perlite improves practical features of plasters, such as workability and covering capacity (consumption). For example, the incorporation of expanded perlite to machine-applied plasters, facilitates the pumping and spraying of the paste and the creation well-finished and levelled surfaces with uniform thickness. The fire behaviour of gypsum is a fundamental property of plasters, but little is known about how the dose of lightweight aggregates as perlite might affect their fire performance. The effect of fire on gypsum plasters reinforced with hemp fibers has been studied by Iucolano et al. [24]. The plasters were heated at 150 °C and 250 °C and the fiber remained relatively well preserved in the matrix despite its combustible nature. After 20 min at 150 °C, the flexural strength was reduced by 38 %, whereas the strength dropped by 65 % in control samples. Besides, the relative proportions of gypsum and bassanite were consistent with the programmed temperatures and heating time. Similarly, Hodhod et al. studied the effectiveness of gypsum plasters made with perlite to provide fire protection to structural elements [25]. After 30 min at 650 °C, gypsum perlite plasters were the best choice for

* Corresponding author.
E-mail address: marcos.lanzon@upct.es (M. Lanzón).

https://doi.org/10.1016/j.conbuildmat.2022.128494
Received 20 April 2022; Received in revised form 11 July 2022; Accepted 13 July 2022
Available online 20 July 2022

protecting RC columns followed by cement vermiculite plasters, those elaborated with expanded clay and, finally, conventional ones. Moreover, the load capacity of the structural elements was not affected by fire when the column was coated with 2.5 cm thickness of perlite plaster, and retained 89.2 % of the initial strength if coated with lower thickness (1.5 cm). Similar studies performed on plasterboard and composites confirm excellent performance of gypsum materials against fire [26–29].

The use of X-ray diffraction (XRD) and thermogravimetric analysis (TG) gives valuable information about the effect of fire on thermally unstable minerals contained in plasters. XRD is a qualitative technique to discriminate gypsum, bassanite and anhydrite in $CaSO_4$ nH_2O mixtures (plasters). However, the relative intensity of the peaks is altered by preferential orientations, the sample preparation method and the morphology of the crystal (habit), which makes XRD quantification more difficult than desired [30]. In contrast, TG analysis provides reliable quantification results if the heating rate, mass of substance and type of crucible are appropriately chosen. Still, gypsum and bassanite dehydration are difficult to distinguish by TG because the weight loss appears overlapped in the thermogram [31,32]. This limitation can be overcome using crucibles covered with perforated lids to create a self-generated atmosphere that improves the separation of the dehydration steps [32]. In this regard, Dunn et al. investigated the effect of self-generated water atmosphere in partially sealed crucibles using DSC analysis to determine the amount of gypsum in cements [33]. They found excellent peak separation between gypsum and hemihydrate using tight seals (0.1 mm and 0.15 mm), although these configurations led to excessive pressure and occasionally the explosion of the crucible. Therefore, openings of 0.20 mm were chosen to avoid these risks because the separation of the peaks (resolution) was also suitable for quantification. The optimal mass of sample (5–35 mg) and heating rate (5–20 °C / min) was 8 mg and 15 °C, respectively and reproducibility tests confirmed the reliability of the method, despite of the small amount of gypsum added to cements (≈ 4–5 %).

This paper aims to study the effect of moderate and high doses of expanded perlite on the fire behaviour of plasters that are compared to control samples. This topic has received little attention in the literature but it is not clear whether the use of high amounts of expanded perlite is beneficial for the protection of plasters and nearby materials of the substrate (e.g. concrete and walls). In this study, IR camera tests and SEM examination are used to show the heat transfer through the plaster and microstructural changes after fire exposure. Finally, XRD, TG and DSC analysis provide additional information about the fire behaviour and dehydration degree of $CaSO_4$ nH_2O minerals in plasters.

2. Materials and methods

2.1. Materials

The binder ($CaSO_4$ $½H_2O$) was supplied by a local manufacturer. It is classified as B1 according to the EN 13279-1 standard, which establishes the technical requirements of construction plasters [34]. Initial XRF analysis confirmed that CaO and SO_3 are the principal oxides as expected for the binder (Table 1). The concentration of H_2O and CO_2 was determined by TG as the technique has greater sensitivity and reliability than XRF for low atomic number elements (low X-ray absorption). XRD confirmed that bassanite and anhydrite were the most abundant minerals in the binder followed by carbonates, gypsum and quartz. The amount of each mineral was semi-quantitatively determined by XRD using DIFFRACT.EVA software based on reference intensity ratio. Table 1 also shows physical properties of expanded perlite along with XRF and XRD analysis. The aggregate principally consists of SiO_2 and Al_2O_3 with minor of alkali metal oxides usually present in igneous rocks.

The plasters were prepared mixing the B1 binder with expanded perlite at doses of 0 %, 2 % and 6.5 % w/w and the resulting samples were coded as M0, P1 and P2, respectively. These percentages were chosen to achieve bulk densities close to 0.800 g/cm^3 and 0.600 g/cm^3 that are similar to low and very low-density plasters available on the market. The samples were compared with control plasters (M0) having a powdered density of 0.942 g/cm^3.

Table 1
Physical-chemical information of binder and expanded perlite.

Physical data	Binder	Expanded perlite
Bulk density, kg/m^3	942	95 ± 5
Grain size, mm	<0.2	0–1.0
Particle geometry	Irregular	Hemi-spherical
Colour	Beige	White - beige
Moisture, %	<0.1	<0.5
Chemical composition, XRF	Binder, %	Expanded perlite, %
H_2O (1)	4.9	1.9
CO_2 (1)	2.5	–
CaO	40.5	1.6
SO_3	49.1	–
SiO_2	1.2	73.3
Al_2O_3	0.4	13.0
MgO	0.8	0.2
Na_2O	–	4.2
K_2O	0.2	4.0
Fe_2O_3	0.2	1.3
SrO	0.2	–
Loss on ignition	–	0.5
Mineral phases, XRD (2)	Binder, %	Expanded perlite, %
Bassanite, $CaSO_4$ ½ H_2O	77.8	–
Anhydrite, $CaSO_4$	11.3	–
Calcite, $CaCO_3$	6.3	–
Dolomite, $CaMg(CO_3)_2$	3.0	–
Gypsum, $CaSO_4$ 2 H_2O	1.0	–
Quartz, SiO_2	0.6	12.8
Albite, $NaSi_3AlO_8$	–	87.2

(1) Concentration determined by TG analysis.
(2) Semi-quantitative determination.

2.2. Methods

2.2.1. Mixing, casting and curing

The amount of mixing water was adjusted to ensure adequate workability of plasters. The mixing process was carried out according to the EN 13279–2 standard [35] using uniform water/solid ratio (w/s = 1.0). After mixing, the pastes were casted in two types of moulds: a) 40 × 40 × 160 mm prismatic moulds for testing mechanical properties and b) squared moulds with dimensions of 200 × 200 × 20 mm necessary to conduct fire tests. Therefore, the latter samples were confectioned with a thickness comparable to that of real plasters (20 mm). The specimens were cured under laboratory conditions (20 ± 3 °C and 65 ± 5 % HR) as recommended by the standard and softly dried at 40 °C one day before performing the tests.

2.2.2. Plasters characterisation: density, hardness, flexural and compressive strength

The density of dry and fresh samples was calculated by dividing the mass of material (±0.01 g) poured into a cylindrical container of known volume (n = 3). As to the hardened material, the edges of the prismatic specimens were measured with a calliper (±0.01 mm) and after that, the mass (±0.01 g) was divided by the apparent volume to obtain their apparent density (n = 3).

Shore-C hardness was tested with a Baxlo® Shore-C durometer equipped with a reference material of 60 Shore-C units. The indentations were made on the lateral sides of the specimens (six per prismatic sample) to avoid possible fluctuations linked to segregation from the bottom to the top part of the specimen. Therefore, a total of 18 Shore-C determinations were obtained for each plaster formulation (M0, P1 and P2).

Finally, flexural and compressive strength tests were conducted as recommended by the EN 13729-2 standard. It is important to stress that the minimal flexural and compressive strength must be 1 MPa and 2 MPa according to the standard. In the flexural tests (three-point tests), the testing machine gives the load necessary to split the prismatic specimens into two sub-samples (n = 3) that were subjected to uniaxial compression tests (n = 6). The mechanical tests were carried out with a Microtest EM2 electromechanical testing machine (±0.01 kN).

2.2.3. Fire tests

The specimens were exposed to fire during 30 min using a propane flame mounted in an adjustable structure equipped with a graduated path. The flame was gradually moved along several positions (0, 1, 2, 3, 4 and 5) and kept in each position for 2, 3, 4, 5, 6 and 10 min, respectively as shown in Fig. 1 [36]. In these conditions, thermographic images of the non-exposed side (NES) were obtained with a FLIR T400 camera to study temperature profile maps at the back side of the plaster and selecting a thermal emissivity coefficient of 0.91 as recommended by the manufacturer. The thermal images were recorded every minute with the camera attached to a tripod in a fixed position and the fire tests were repeated three times per sample (M0, P1 and P2). After completing the tests, small fragments were carefully removed from the region directly exposed to fire (exposed side) and the back side of the plaster (non-exposed side). The sampling area was restricted to 2.5–3 cm^2 to ensure the reliability of further analyses. Once removed, the fragments were grounded to a fine powder using a pestle and mortar, introduced into hermetically sealed plastic bags and stored into a desiccator to prevent rehydration to happen.

2.2.4. Scanning electron microscopy examination (SEM)

SEM images were captured for unfired samples and those exposed to fire. In the fired samples, the two sides of the specimens i.e. the exposed side (ES) and non-exposed side (NES) were examined by SEM. The analyses were carried out with a Hitachi S-3500N scanning electron microscope at a voltage of 15 kV at variable magnification (100–2000) in Backscattered Electrons mode (BSE).

2.2.5. X-ray diffraction analysis (XRD)

Gypsum ($CaSO_4$ $2H_2O$) is progressively transformed into basanite ($CaSO_4$ $½H_2O$) and anhydrite ($CaSO_4$) by heating. Hence, XRD provides useful information on the existence of the formed minerals depending on the achieved temperature in plasters exposed to fire. The analyses were conducted in unfired plasters and also in fragments removed from the exposed side (ES) and non-exposed side (NES) of M0, P1 and P2 plasters. The samples were gently ground in a mortar and the mineral phases were identified using Cu K-alpha line X-ray emission with a Bruker D8 Advance powder diffractometer for powder analysis. The selected scan angle range (2-theta) varied from 10° to 70° with a resolution of 0.05°. The analysis was performed with DIFFRAC.EVA software (version 4.0) that allows peaks smoothing correction, Kα2-stripping, automatic background subtraction, calculation of crystallinity degree and semi-quantitative analysis of mineral phases.

2.2.6. Thermogravimetric analysis (TG)

Unfired specimens and fragments taken from the ES and NES of plasters subjected to fire were studied by TG analysis to obtain quantitative information about the dehydration degree of $CaSO_4$ nH_2O minerals present in plasters. The samples were heated at 60 °C for 24 h to remove possible rests of free water before performing TG measurements. A Mettler-Toledo TGA / DSC HT thermogravimetric analyser was used and the temperature was progressively increased from room temperature to 1000 °C with an accuracy of ± 0.5 °C. Alumina crucibles containing approximately 10 mg of sample were used in the analysis with a heating rate of 10 °C/min in N_2 atmosphere and a flow rate of 50 ml/min.

2.2.7. Differential scanning calorimetry (DSC)

The plasters were also studied by differential scanning calorimetry using a Metter-Toledo DSC 822E calorimeter. To reduce the influence of sample preparation as much as possible, all measurements were made in the same conditions. First, 5 mg of sample were weighed in a microbalance (±0.000001 g) using 40 μL aluminium crucibles, which were covered with micro-perforated lids (50 μm). After that, the samples were carefully pressed down to the bottom of the crucible using a plunger in order to improve the heat transfer through the sample and the reliability of DSC measurements (Fig. 2a). A Mettler-Toledo sealing press was used to seal hermitically the crucible with the lid producing a cold-welded union (Fig. 2b). The lid increases the internal vapour pressure due to self-generated atmosphere inside the crucible (Fig. 2c).

In these conditions, the endothermic peaks resulting from gypsum (1) and bassanite (2) dehydration are better separated in the thermogram:

$$CaSO_4\ 2H_2O \rightarrow CaSO_4\ 0.5H_2O + 1.5\ H_2O \quad (1)$$

$$CaSO_4\ 0.5H_2O \rightarrow CaSO_4 + 0.5\ H_2O \quad (2)$$

The area of the endothermic peaks (J/g) was used to evaluate the quantity of gypsum (1) and/or bassanite (2) after fire exposure. The experiments were performed at 5 °C/min from 25 °C to 250 °C in N_2 at 20 ml/min and standard calibration curves were confectioned using calcium sulphate dihydrate (gypsum) and hemihydrate (bassanite) provided by Sigma Aldrich.

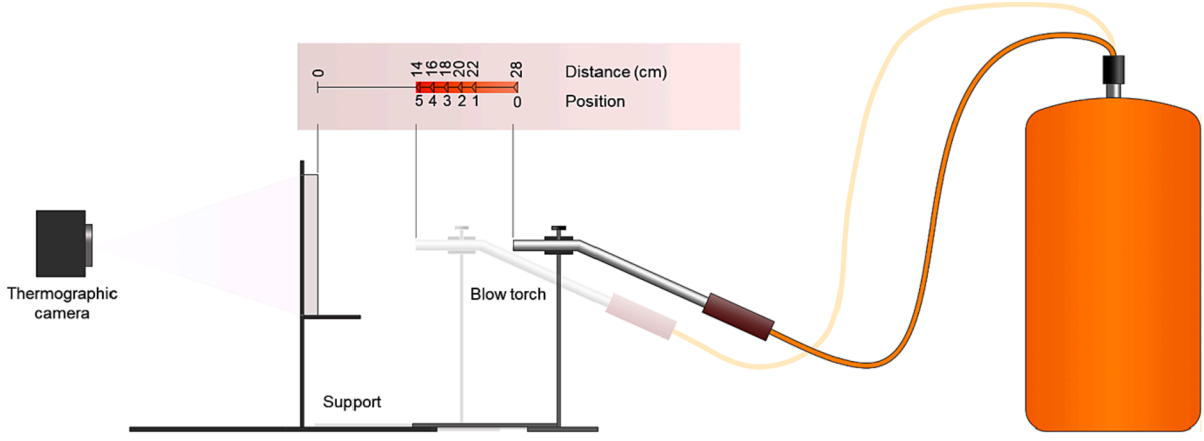

Fig. 1. Diagram of the direct fire test components.

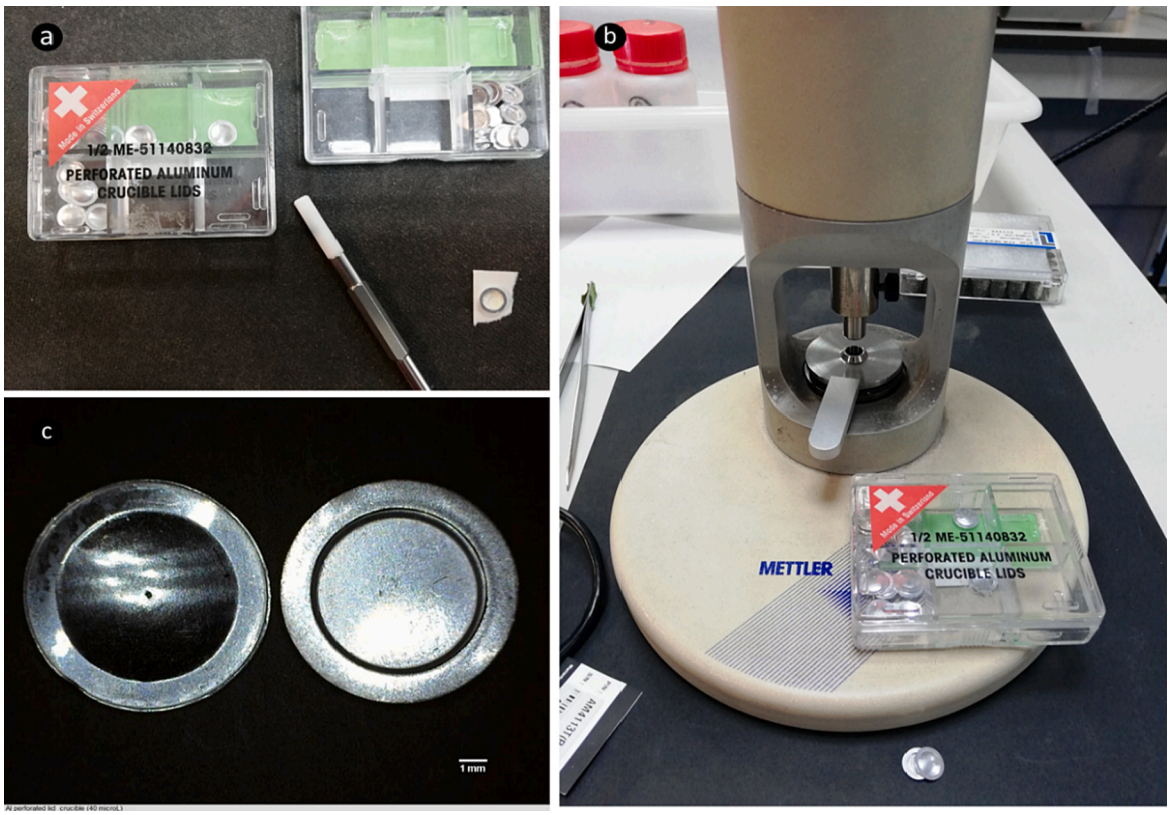

Fig. 2. Steps and tools used for DSC analysis; a) sample preparation with manual plunger; b) sealing press for confining the sample; c) detail of 40 μL aluminium crucible and micro-perforated lid.

3. Results and discussion

3.1. Physical characterisation of plasters: density, hardness and mechanical strength

The effect of expanded perlite on powder, fresh and hardened density is shown in Table 2. The density of M0 and P1 samples is comparable to that of plasters available on the market. As seen from the table, the mechanical performance of plasters made with moderate doses of expanded perlite (P1) and control samples (M0) is rather similar. By contrast, high doses of expanded perlite (P2) led to considerable drop of flexural and compressive strength, and the mechanical resistance was reduced by around 20 % if compared to control samples. Nevertheless, the plasters meet the requirements of the EN 13,279 standard, by which flexural and compressive strength must exceed 1 MPa and 2 MPa, respectively. The hardness values were moderately affected by the incorporation of perlite and the Shore C dropped by 5.4 % and 12.8 % in lightweight plasters.

Table 2
Density, Shore C hardness and mechanical strength of plasters.

Mix code.	Powder density, g/cm^3	Fresh density, g/cm^3	Hardened density, g/cm^3
M0	0.942	1.415	0.843
P1	0.800	1.318	0.791
P2	0.600	1.155	0.729

Mix code.	Shore C, units (n = 18)	Flexural strength, MPa (n = 3)	Compressive strength, MPa (n = 6)
M0	57.7 ± 0.7	1.83 ± 0.16	4.80 ± 0.17
P1	54.6 ± 1.5	1.82 ± 0.03	4.55 ± 0.18
P2	50.3 ± 0.5	1.46 ± 0.10	3.69 ± 0.15

3.2. Fire tests

This section aims to evaluate the effect of expanded perlite in the composition of the plaster, especially in the back side where building materials like concrete or renders are usually placed. Fig. 3 shows the temperature variation (n = 3) recorded by the thermographic camera in the non-exposed side (NES) of plasters throughout 30 min. The camera allows acquisition of average and maximum temperatures over the entire surface. The relative standard deviation (RSD) for the average and maximum temperature data was lower than 5 % throughout the experiment (30 min), although higher fluctuations were observed during the first 5 min (RSD < 10 %). However, in the last part of the experiment (25–30 min), where more stable conditions were achieved, this fluctuation was found to be 2–3 %. As can be seen, little differences were found for the average temperature of M0 and P2 plasters (top) that behave similarly throughout the experiment. However, P1 samples showed better fire performance than M0 and P2 and the differences were more remarkable along time. The maximum temperature in the back side of plasters was found along the longitudinal axis of the flame due to radial heat propagation. In this case, the maximum temperature increased sharply in P2 samples after 25 min of fire exposure (bottom; red line). This may indicate that the use of excessive amounts of perlite creates added channels and defects in the matrix through which heat may be transferred in a more efficient manner. In addition, P2 samples were mechanically more fragile than M0 or P1 and the occurrence of cracks during the test could facilitate the heat transfer as well.

Temperature maps recorded by the IR camera corroborated the same behaviour (Fig. 4). IR images captured at the non-exposed side after 5, 10, 20, 25 and 30 min, illustrate clearly what happens 2 cm underneath the plaster where other building materials are placed. The heat transmission was somewhat similar within the initial time interval (5–20 min), although greater differences were observed during the final interval (25–30 min). At 30 min, the effect of fire was visibly focalised in

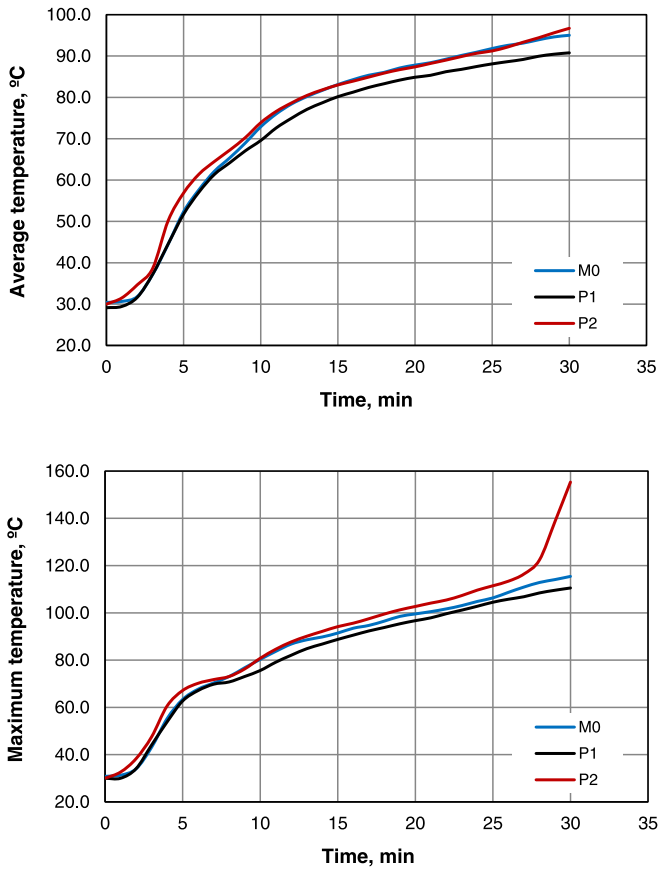

Fig. 3. Average and maximum temperature in the back side of plasters exposed to fire; three determinations were made per sample (n = 3).

the flame action zone leading to maximum temperatures between 108.7 and 167.7 °C in that area. As seen in the figure, plasters containing moderate doses of expanded perlite (P1) provided cooler temperatures at any time exposure and once again, the highest heat transmission was observed in P2 plasters. As said before, the heat pattern diffusion observed in P2 is likely related to lower mechanical strength and deficient bonding between perlite and the gypsum matrix.

3.3. Scanning electron microscopy (SEM) analysis

The distribution of expanded perlite grains in gypsum plasters is shown at several magnifications in Fig. 5. The large range size of perlite grains allows visualisation from low magnifications as shown Fig. 5a. The perlite aggregates ranged in size from millimetric scale to hundreds or dozens of micrometres (Fig. 5b-c), but some particles had sizes below 10 μm (Fig. 5d). In addition to usual segregation issues observed in lightweight aggregates, it was found that the perlite grains were not strongly adhered to the binding phase of gypsum (Fig. 5a, b and c).

Fig. 6 shows M0, P1 and P2 plasters before and after being exposed to fire at the same magnification (×2000). Before fire exposure, usual habits of gypsum consisting of acicular, tabular, prismatic and twined shapes were observed in SEM (Fig. 6a-c). The action of fire led to smaller and thinner crystals having more elongated shapes (Fig. 6d-i) that are slightly different from those shown in samples not exposed to fire (Fig. 6a-c). In this case, twined shapes were not distinguished and the majority of crystals had fibrous forms, especially in P2 plasters and in the side directly exposed to fire (red arrows indicate expanded perlite grains). These morphological changes are explained by gypsum conversion into dehydrated minerals exhibiting different habits.

3.4. X-ray diffraction analysis (XRD)

XRD tests were performed to study the main minerals present in M0, P1 and P2 before and after conducting fire tests (Fig. 7). To improve the readability of the diffractograms, minor components like calcite, dolomite and quartz were not labelled in the figures. In unfired M0 samples

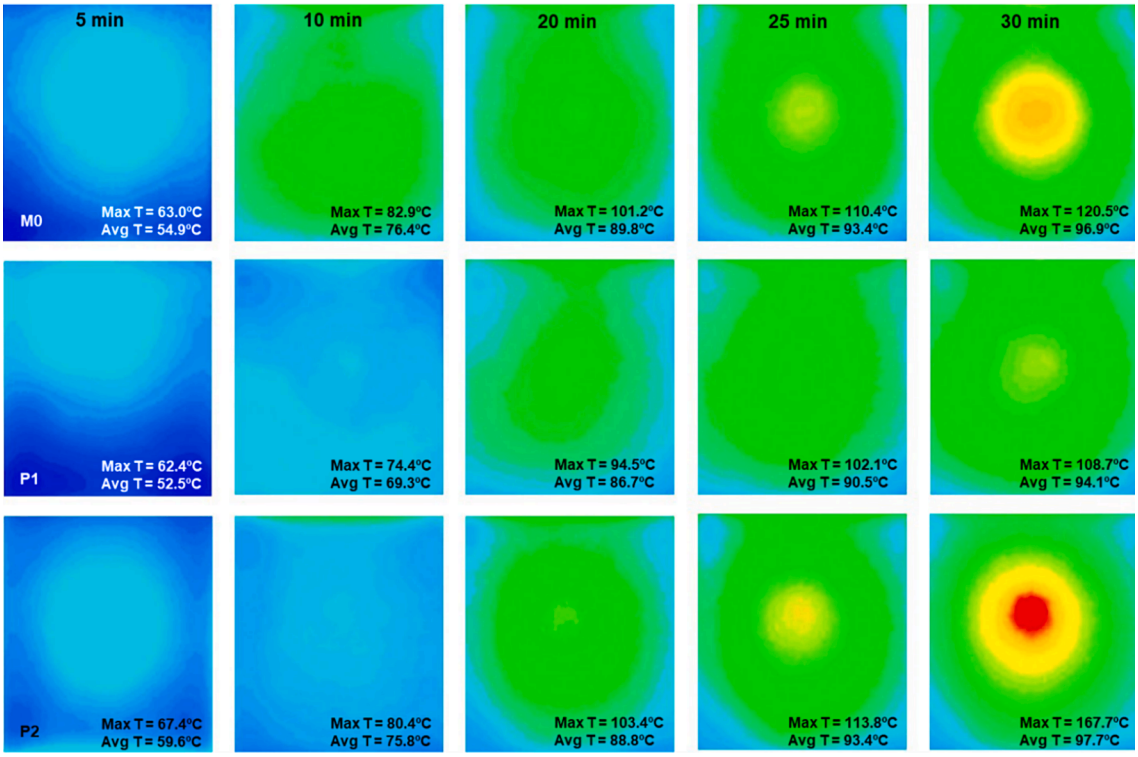

Fig. 4. Temperature maps in the non-exposed side of plasters (M0, P1 and P2) within 5–30 min.

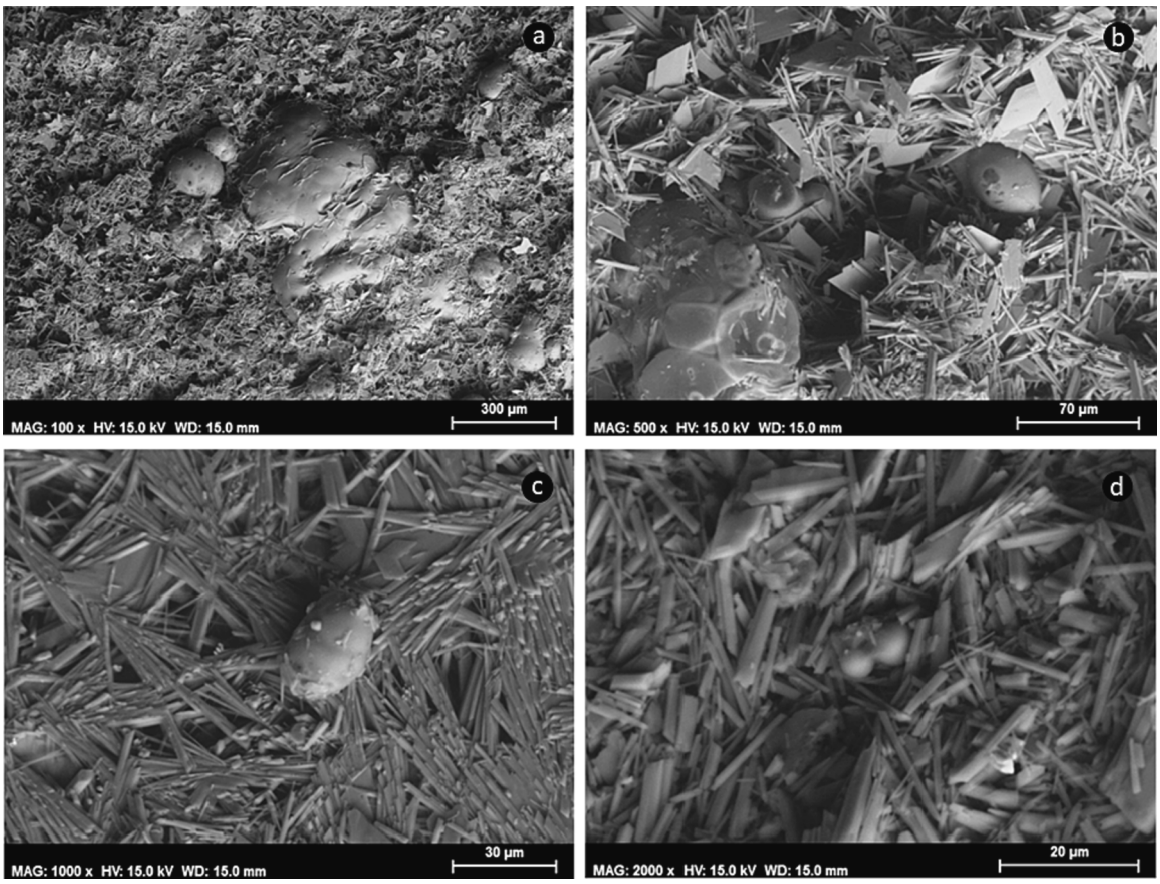

Fig. 5. Microstructural details of plasters containing expanded perlite at ×100; ×500; ×1000 and ×2000.

(blue line), gypsum ($CaSO_4$ $2H_2O$) was the main constituent as shown Fig. 7 top. The heating action of the flame provoked important variations in the exposed side (ES) and gypsum was completely converted into anhydrite ($CaSO_4$). In the non-exposed side of M0 plasters (NES), bassanite was the predominant form, but the existence of gypsum was negligible.

In P1 plasters, gypsum was the major mineral in unfired samples (blue line; Fig. 7 centre). However, the non-exposed side of P1 (black line) seems to be little affected by fire, which may indicate better preservation of P1 (NES) in relation to M0 (NES). In fact, the main signals are attributed to gypsum, while the contribution of bassanite and anhydrite, if any, was found to be minimal in the NES of P1. Finally, the fire action caused total dehydration of sulphate minerals located in the exposed side (ES). In P2, as found for M0 and P1, anhydrite was the principal component in the side directly exposed to fire (red line; Fig. 7 bottom). In this instance, the non-exposed side showed greater alteration than P1 (NES) and gypsum was replaced by bassanite (black line). The detection of bassanite in P2 is consistent with the maximum temperature of 167.7 °C recorded by IR camera measurements in the NES. This temperature is enough for transforming $CaSO_4$ $2H_2O$ into the hemihydrate, but not enough to achieve complete dehydration ($CaSO_4$). Thus, XRD analyses confirm that the incorporation of high quantities of expanded perlite may facilitate the heat transfer through the plaster.

3.5. Thermogravimetric analysis (TG)

TG allows quantitative assessment of thermally labile components like water, which is often chemically bonded to sulphates ($CaSO_4$ nH_2O). In this case, the higher plaster stability to fire, the greater weight loss due to remaining water molecules in $CaSO_4$ nH_2O crystals. As confirmed by XRD (blue line; Fig, 7), the magnitude of the weight loss between 130 and 180 °C confirms that gypsum is the most abundant mineral in unfired samples due to bassanite hydration (blue line; Fig. 8 top, centre and bottom). The first step of the thermogram is related to water release (18.0147 g/mol) from gypsum $CaSO_4$ $2H_2O$ (172.17 g/mol), which entails a stoichiometric weight loss of 20.9746 %. Thus, the concentration of gypsum in unfired plasters M0, P1 and P2 was 92.48 %, 91.05 % and 87.90 %, respectively.

The TG curves also confirmed that the non-exposed side of plasters (black line) was affected in a different manner depending on their composition. For example, in P1 the weight loss of 18.9756 % (Fig. 8; centre) indicates the material was altered to a lesser extent than M0 and P2. The weight loss in P1 was about three times greater than that of M0 and P2 indicating better preservation of the former plaster. This result is consistent with previous XRD analysis because gypsum was the main mineral in the non-exposed side of P1. Instead, the exposed side of the plasters (red line) was strongly affected by fire and the small percentage of water is explained by residual moisture in the samples. The severity of fire in the exposed side (ES) is also visible from the drop of the second step associated to carbonates when compared to unfired plasters and the non-exposed side of plasters (NES).

Table 3 provides a summary of identified species in both unfired plasters and plasters subjected to fire. In unfired samples (M0, P1 and P2), gypsum is undoubtedly the substance responsible for the first step of the thermogram. However, in the non-exposed side of M0, P1 and P2 samples – coded as M0 (NES), P1 (NES) and P2 (NES) – the quantification is much more difficult as explained before. In M0 (NES) and P2 (NES), bassanite was found to be the main mineral according to XRD data and hence, the TG quantification has been done assuming negligible contribution of gypsum to the first step of the thermogram. Likewise, as confirmed by XRD, in P1 (NES) the major contribution to the weight loss between 130 and 180 °C is due to gypsum (Fig. 8; centre).

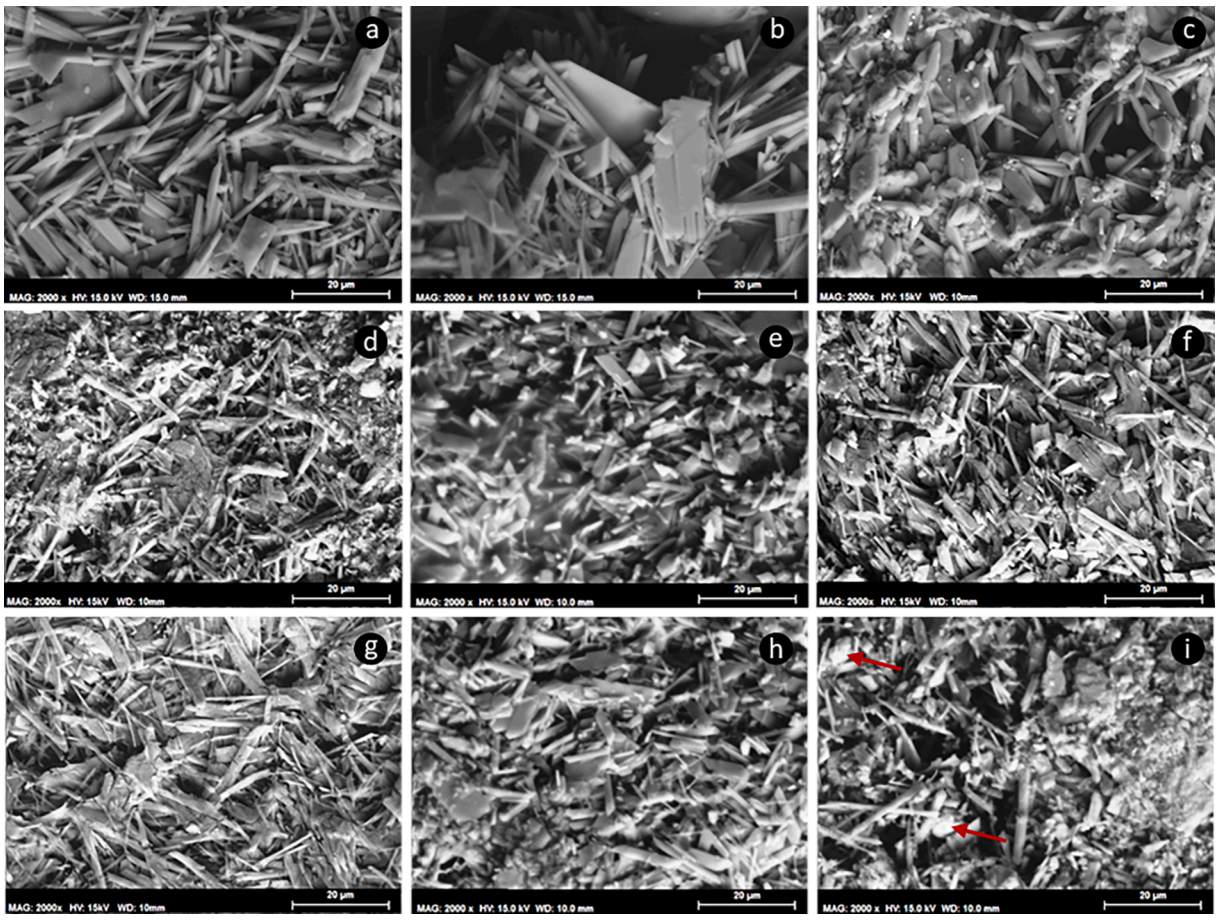

Fig. 6. SEM examination (×2000) of gypsum plasters; a), b) and c) M0, P1 and P2 plasters before fire exposure; d), e) and f) non-exposed side of M0, P1 and P2 samples; g), h) and i) side directly exposed to fire in M0, P1 and P2 samples.

The XRD and TG results match well despite inherent limitations of XRD for quantitative analysis of gypsum [30].

3.6. Differential scanning calorimetry (DSC)

DSC analysis was conducted to discriminate gypsum from bassanite in the non-exposed side to fire and also to verify the stated assumptions for TG analysis. Here, the use of pinhole lids (50 μm) allowed effective separation of gypsum and bassanite signals (peaks) to overcome a common limitation of TG. Fig. 9 shows the thermogram of standard calcium sulphate dihydrate (purity > 99.8 %) with two well-resolved peaks at about 140 °C and 190 °C. The first peak is due to endothermic release of 1.5 water molecules from $CaSO_4\ 2H_2O$ and the second one occurs by removal of the remaining 0.5 water molecules from bassanite ($CaSO_4\ ½H_2O$).

The concentration of gypsum and bassanite in M0, P1 and P2 plasters was determined from the area of the first and second peak using calibration curves and linear regression analysis ($r^2 > 0.99$). The calibration was carried out with standard calcium sulphate dihydrate and hemihydrate by plotting the area (J/g) of the corresponding peaks as a function of gypsum and bassanite concentration (%). It is worth noting that the second peak is contributed by gypsum because $CaSO_4\ 2H_2O$ dehydration leads to secondary bassanite ($CaSO_4\ ½H_2O$) in addition to initial bassanite that might be already present in the sample. Hence, the contribution of gypsum was subtracted from the total area of the second peak to avoid an overestimation of bassanite [33]. The temperature intervals and integration criteria for the samples and calibration tests were kept uniform for comparative purposes.

DSC analysis confirmed that gypsum was a minor mineral in M0 and P2 samples (4.61 % and 2.34 %), while bassanite was the principal component in these samples (89.4 % and 92.68 %). Equally, in P1 samples the concentration of gypsum in the non-exposed side was 91.27 % and the bassanite content was below 1 %. To conclude, the chosen DSC approach allowed discrimination of bassanite and gypsum in plasters subjected to fire and the results confirm that expanded perlite may decrease the plaster fire protection, especially if used in high doses.

4. Conclusions

The combination of the proposed techniques (IR maps, SEM, XRD, TG and DSC) provide valuable information about the effect of fire on key minerals of plasters as well as possible damage of materials directly in contact with the plaster (e.g. substrate). In more detail, the following conclusions can be drawn from the results of the study:

- The use of expanded perlite is a highly effective way to produce lightweight plasters. The mechanical strength and hardness are not significantly affected by moderate amounts of expanded perlite (2.0 % w/w). In contrast, the flexural and compressive strength are significantly reduced adding high quantity of perlite (6.5 % w/w). Despite the above, all plasters conform the mechanical requirements of the EN 13279 standard regardless the expanded perlite content.
- IR maps also reveal a higher heat transfer and temperature when high doses of expanded perlite are used. SEM examination shows limited bonding between expanded perlite grains and the gypsum matrix. The lack of physical bonding between perlite and gypsum may explain the strength reduction, and also facilitate the occurrence

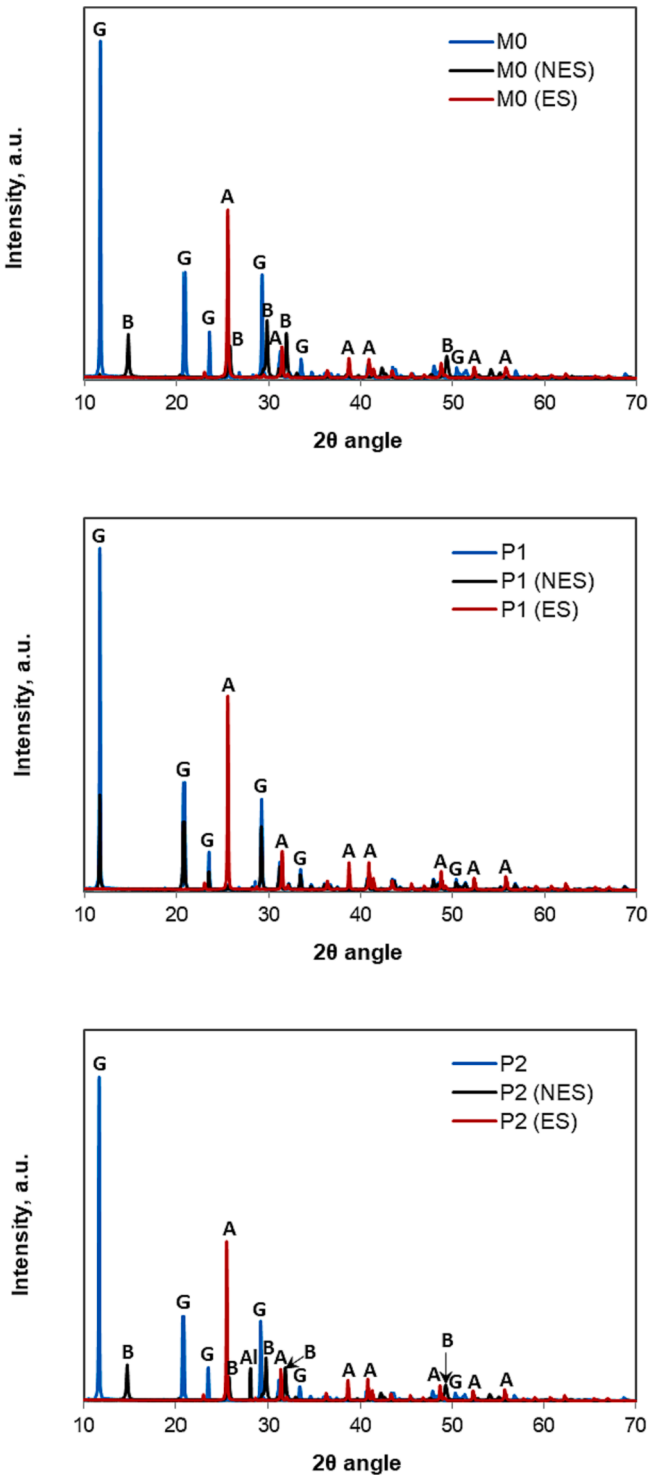

Fig. 7. XRD patterns of M0 (top), P1 (centre) and P2 (bottom) plasters before and after fire testing; G = gypsum; B = bassanite; A = anhydrite; Al = albite.

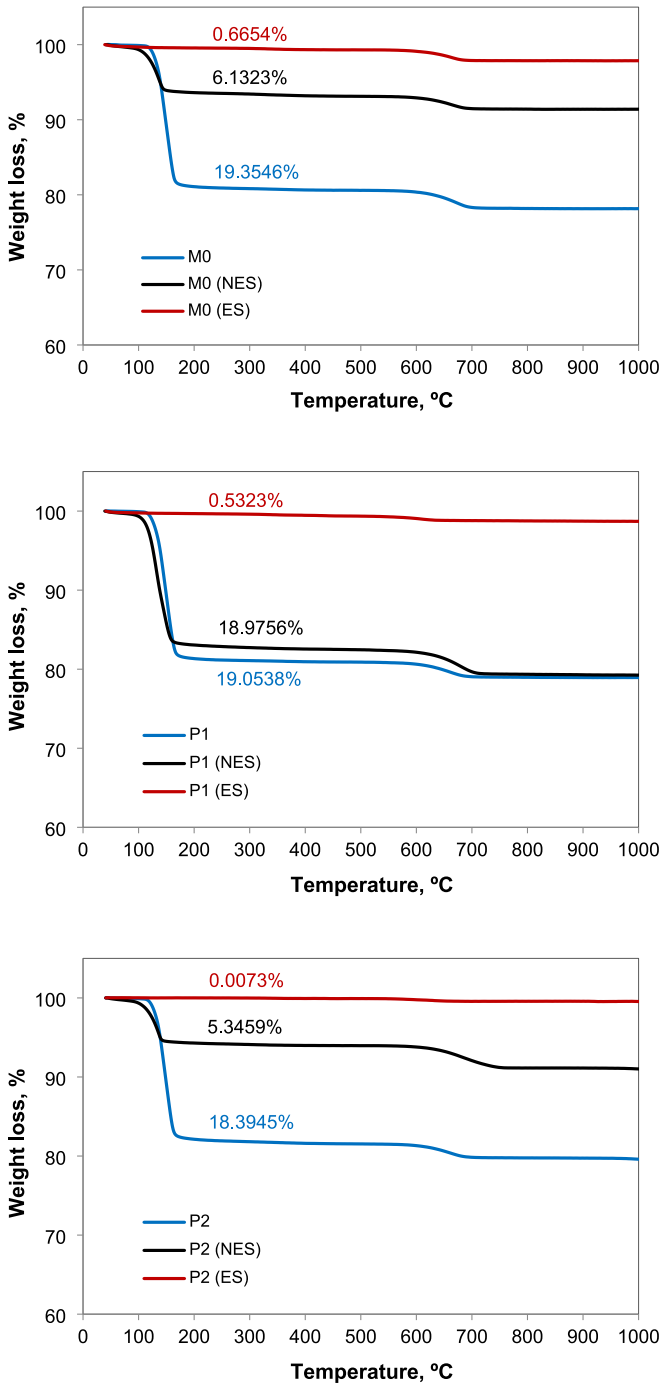

Fig. 8. TG analysis and water release (%) from M0 (top) P1 (centre) and P2 (bottom) plasters.

of further micro-structural defects through which heat may be transferred, as seen by the IR images.

- The XRD analysis of samples subjected to fire shows important differences between the external and internal side of the plaster (i.e. the exposed and non-exposed side). After 30 min of fire exposure, plasters elaborated with moderate doses of perlite remain well preserved and gypsum ($CaSO_4$ $2H_2O$) is the predominant mineral in the plaster back side. By contrast, control samples and samples containing high doses of perlite present high content of bassanite ($CaSO_4$ $½H_2O$) which denotes further alteration of the plaster. The severity of fire is especially visible in the side directly exposed to fire since gypsum and bassanite are completely transformed into anhydrite regardless the dose of perlite.
- The damage caused by fire can be quantified by TG analysis using the water release from $CaSO_4$ nH_2O structures. The water weight loss gives valuable information on the plater's resistance to fire, which is about three times greater in samples containing moderate doses of perlite (P1). An important limitation of TG is that the dehydration of gypsum and bassanite occurs at similar temperatures making their quantification much more difficult. Though, when gypsum or bassanite are the most abundant forms, the weight loss can be assigned

Table 3
Minerals quantification: TG and XRD comparison.

Sample M0	**M0**	**M0 (NES)**	**M0 (ES)**
Crystallisation water loss ($CaSO_4$ nH_2O), %	19.3546	6.1323	0.6654
Main mineral found by XRD	Gypsum	Bassanite	Anhydrite
Stoichiometric weight loss, %	20.93	6.21	–
TG quantification, %	92.48	98.75	–
XRD evaluation, %	84.8	90.5	96.9
Sample P1	**P1**	**P1 (NES)**	**P1 (ES)**
Crystallisation water loss ($CaSO_4$ nH_2O), %	19.0538	18.9756	0.5323
Main mineral found by XRD	Gypsum	Gypsum	Anhydrite
Stoichiometric weight loss, %	20.93	20.93	–
TG quantification, %	91.05	90.66	–
XRD evaluation, %	91.5	90.2	98.9
Sample P2	**P2**	**P2 (NES)**	**P2 (ES)**
Crystallisation water loss ($CaSO_4$ nH_2O), %	18.3945	5.3459	0.0007
Main mineral found by XRD	Gypsum	Bassanite	Anhydrite
Stoichiometric weight loss, %	20.93	6.21	–
TG quantification, %	87.90	86.15	–
XRD evaluation, %	91.6	95.5	98.9

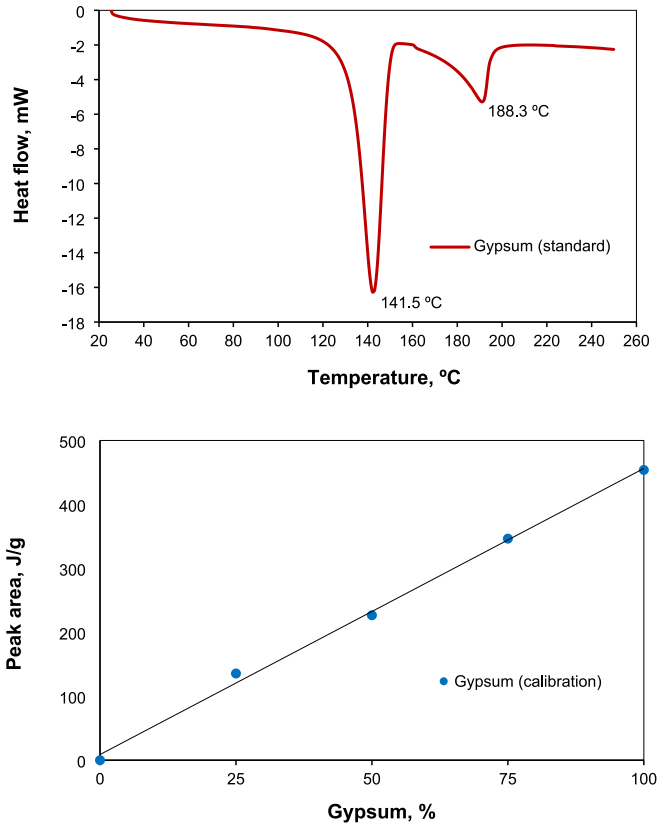

Fig. 9. Top: DSC heat flow curve with appropriate separation (resolution) of gypsum and bassanite signals; Bottom: calibration curve for quantification.

with little error to either of them. For this purpose, previous XRD information can be used to validate this assumption.

- The use of perforated lids in DSC analysis allows appropriate separation of endothermic signals resulting from gypsum and bassanite dehydration. Thus, the content of gypsum and bassanite can be measured with much better accuracy than that achieved by TG analysis. Nevertheless, DSC and TG analysis yield comparable results that are in good agreement with XRD data.
- An important conclusion of the study is that moderate doses of expanded perlite (2.0 % w/w) are highly effective to protect plasters against fire, whereas high percentages of perlite (6.5 % w/w) may have a detrimental effect on fire performance. Although further studies are necessary to elucidate the role of expanded perlite in lightweight plasters subjected to fire, it is clear that the dose of perlite can be a crucial factor. Finally, the influence of the coating's thickness and the damage caused by fire in materials coated with perlite plasters are worth exploring in future research as well as the dose of expanded perlite above which fire performance starts to decrease or it is not sufficiently achieved.

CRediT authorship contribution statement

Marcos Lanzón: Methodology, Formal analysis, Writing – original draft, Writing – review & editing, Visualization, Supervision, Funding acquisition. **Francisco José Castellón:** Conceptualization, Investigation, Resources, Writing – original draft, Validation, Funding acquisition. **Manuel Ayala:** Investigation, Resources.

Declaration of Competing Interest

The authors declare that they have no known competing financial interests or personal relationships that could have appeared to influence the work reported in this paper.

Data availability

Data will be made available on request.

Acknowledgments

The support given by the Technical University of Cartagena, UPCT is greatly appreciated (Ref: 3005216651; D023-09: Advanced mortars for building and architectural restoration). The authors want also to express their gratitude to Vicente Muñoz and Alberto Alcolea from SAIT laboratory at UPCT, who help us to overcome practical limitations of thermal analysis.

References

[1] European Committee for Standardization (CEN), EN 13501-1:2019. Fire classification of construction products and building elements - Part 1: Classification using data from reaction to fire tests.
[2] M. Doleželová, L. Scheinherrová, J. Krejsová, M. Keppert, R. Černý, A. Vimmrová, Investigation of gypsum composites with different lightweight fillers, Constr. Build. Mater. 297 (2021), 123791, https://doi.org/10.1016/j.conbuildmat.2021.123791.
[3] M. Doleželová, L. Scheinherrová, J. Krejsová, A. Vimmrová, Effect of high temperatures on gypsum-based composites, Constr. Build. Mater. 168 (2018) 82–90, https://doi.org/10.1016/j.conbuildmat.2018.02.101.
[4] M. Alaa, Rashad, A synopsis about perlite as building material – A best practice guide for Civil Engineer (review), Constr. Build. Mater. 121 (2016) 338–353, https://doi.org/10.1016/j.conbuildmat.2016.06.001.
[5] S. Bakhtiyari, A. Allahberdi, M. Rais-Ghasemi, A case study on modifying the fire resistance of self-compacting concrete with expanded perlite aggregate and zeolite powder additives, Asian J. Civil Eng. 15 (2014) 339–349.
[6] I. Türkmen, A. Kantarci, Effects of expanded perlite aggregate and different curing conditions on the physical and mechanical properties of self-compacting concrete, Build. Environ. 42 (2007) 2378–2383, https://doi.org/10.1016/j.buildenv.2006.06.002.
[7] S. Abidi, Y. Joliff, C. Favotto, Impact of perlite, vermiculite and cement on the Young modulus of a plaster composite material: Experimental, analytical and numerical approaches, Compos. B Eng. 92 (2016) 28–36, https://doi.org/10.1016/j.compositesb.2016.02.034.
[8] H. Oktay, R. Yumrutas, A. Akpolat, Mechanical and thermophysical properties of lightweight aggregate concretes, Constr. Build. Mater. 96 (2015) 217–225, https://doi.org/10.1016/j.conbuildmat.2015.08.015.
[9] R. Demirboga, I. Örüng, R. Gül, Effects of expanded perlite aggregate and mineral admixtures on the compressive strength of low-density concretes, Cem. Concr. Res. 31 (2001) 1627–1632, https://doi.org/10.1016/S0008-8846(01)00615-9.
[10] O. Sengul, S. Azizi, F. Karaosmanoglu, M.A. Tasdemir, Effect of expanded perlite on the mechanical properties and thermal conductivity of lightweight concrete, Energy Build. 43 (2011) 671–676, https://doi.org/10.1016/j.enbuild.2010.11.008.

[11] D. Kramar, V. Bindiganavile, Impact response of lightweight mortars containing expanded perlite, Cem. Concr. Compos. 37 (2013) 205–214, https://doi.org/10.1016/j.cemconcomp.2012.10.004.
[12] H. Shoukry, M.F. Kotkata, S.A. Abo-El-Enein, M.S. Morsy, S.S. Shebl, Thermo-physical properties of nanostructured lightweight fiber reinforced cementitious composites, Constr. Build. Mater. 102 (2016) 167–174, https://doi.org/10.1016/j.conbuildmat.2015.10.188.
[13] M. Lanzón, P.A. García-Ruiz, Lightweight cement mortars: Advantages and inconveniences of expanded perlite and its influence on fresh and hardened state and durability, Constr. Build. Mater. 22 (2008) 1798–1806, https://doi.org/10.1016/j.conbuildmat.2007.05.006.
[14] V. Brunello, D. Bersani, L. Rampazzi, A. Sansonetti, C. Tedeschi, Gypsum based mixes for conservation purposes: evaluation of microstructural and mechanical features, Materiales de Construcción 70 (2020), e207, https://doi.org/10.3989/mc.2020.05019.
[15] T.K. Erdem, Ç. Meral, M. Tokyay, T.Y. Erdogan, Use of perlite as a pozzolanic addition in producing blended cements, Cem. Concr. Compos. 29 (2007) 13–21, https://doi.org/10.1016/j.cemconcomp.2006.07.018.
[16] L.-H. Yu, H. Ou, L.-L. Lee, Investigation on pozzolanic effect of perlite powder in concrete, Cem. Concr. Res. 33 (2003) 73–76, https://doi.org/10.1016/S0008-8846(02)00924-9.
[17] A.A. Ramezanianpour, S. Mahmoud Motahari Karein, Payam Vosoughi Amirreza Pilvar Soroush Isapour, Faramarz Moodi, Effects of calcined perlite powder as a SCM on the strength and permeability of concrete, Constr. Build. Mater. 66 (2014) 222–228, https://doi.org/10.1016/j.conbuildmat.2014.05.086.
[18] M. Lanzón, P.A. García-Ruiz, Lightweight pozzolanic materials used in mortars: Evaluation of their influence on density, mechanical strength and water absorption, Cem. Concr. Compos. 31 (2009) 114–119, https://doi.org/10.1016/j.cemconcomp.2008.11.003.
[19] S.T. Erdoğan, A.Ü. Sağlık, Early-age activation of cement pastes and mortars containing ground perlite as a pozzolan, Cem. Concr. Compos. 38 (2013) 29–39, https://doi.org/10.1016/j.cemconcomp.2013.03.004.
[20] İ.B. Topçu, B. Işıkdağ, Manufacture of high heat conductivity resistant clay bricks containing perlite, Build. Environ. 42 (2007) 3540–3546, https://doi.org/10.1016/j.buildenv.2006.10.016.
[21] M.S. Morsy, H.A. Aglan, Development and characterization of nanostructured-perlite-cementitious surface compounds, J. Mater. Sci. 42 (2007) 10188–10195, https://doi.org/10.1007/s10853-007-1981-3.
[22] R. Demirboğa, R. Gül, The effects of expanded perlite aggregate, silica fume and fly ash on the thermal conductivity of lightweight concrete, Cem. Concr. Res. 33 (2003) 723–727, https://doi.org/10.1016/S0008-8846(02)01032-3.
[23] S. Abidi, B. Nait-Ali, Y. Joliff, C. Favotto, Impact of perlite, vermiculite and cement on the thermal conductivity of a plaster composite material: Experimental and numerical approaches, Compos. B Eng. 68 (2015) 392–400, https://doi.org/10.1016/j.compositesb.2014.07.030.
[24] F. Iucolano, B. Liguori, P. Aprea, D. Caputo, Thermo-mechanical behaviour of hemp fibers-reinforced gypsum plasters, Constr. Build. Mater. 185 (2018) 256–263, https://doi.org/10.1016/j.conbuildmat.2018.07.036.
[25] O.A. Hodhod, A.M. Rashad, M.M. Abdel-Razek, A.M. Ragab, Coating protection of loaded RC columns to resist elevated temperature, Fire Saf. J. 44 (2009) 241–249, https://doi.org/10.1016/j.firesaf.2008.06.010.
[26] L. Zhang, Y. Dai, Y. Bai, W. Chen, J. Ye, Fire performance of loaded fibre reinforced polymer multicellular composite structures with fire-resistant panels, Constr. Build. Mater. 296 (2021), 123733, https://doi.org/10.1016/j.conbuildmat.2021.123733.
[27] D.I. Kolaitis, E.K. Asimakopoulou, M.A. Founti, Fire behaviour of gypsum plasterboard wall assemblies: CFD simulation of a full-scale residential building, Case Stud Fire Safety 7 (2017) 23–35, https://doi.org/10.1016/j.csfs.2016.11.001.
[28] A. Ciudad, A.M. Lacasta, L. Haurie, J. Formosa, J.M. Chimenos, Improvement of passive fire protection in a gypsum panel by adding inorganic fillers: Experiment and theory, Appl. Therm. Eng. 31 (2011) 3971–3978, https://doi.org/10.1016/j.applthermaleng.2011.07.048.
[29] C. Martias, Y. Joliff, C. Favotto, Effects of the addition of glass fibers, mica and vermiculite on the mechanical properties of a gypsum-based composite at room temperature and during a fire test, Compos. B Eng. 62 (2014) 37–53, https://doi.org/10.1016/j.compositesb.2014.02.019.
[30] M. Inoue, I. Hirasawa, The relationship between crystal morphology and XRD peak intensity on $CaSO_4{\cdot}2H_2O$, J. Cryst. Growth 380 (2013) 169–175, https://doi.org/10.1016/j.jcrysgro.2013.06.017.
[31] J.R. Clifton, Thermal analysis of calcium sulfate dihydrate and supposed α and β forms of calcium sulfate hemihydrate from 25 to 500 °C, Journal of Research of the National Bureau of Standards – A, Physics and Chemistry 76A (1972) 41–49, https://doi.org/10.6028/jres.076A.005.
[32] M. Földvári, Handbook of Thermogravimetric System of Minerals and its Use in Geological Practice, Occasional Papers of Geological Institute of Hungary, Budapest, 2011.
[33] J. Dunn, K. Oliver, G. Nguyein n, I. Sills, The quantitative determination of hydrated calcium sulphates in cement by DSC, Thermochim. Acta 121 (1987) 181–191, https://doi.org/10.1016/0040-6031(87)80170-3.
[34] European Committee for Standardization (CEN), EN 13279-1:2009. Gypsum binders and gypsum plasters – Part 1: Definitions and requirements.
[35] European Committee for Standardization (CEN), EN 13279-2:2014. Gypsum binders and gypsum plasters – Part 1: Tests methods.
[36] F.J. Castellón, M. Ayala, J.A. Flores, M. Lanzón, Influence of citric acid on the fire behavior of gypsum coatings of construction and structural elements, Mater. Construcción 71 (2021), e248, https://doi.org/10.3989/mc.2021.13120.